AGU100 ADVANCING EARTH AND SPACE SCIENCE

Geophysical Research Letters

RESEARCH LETTER
10.1029/2018GL077799

Key Points:
- The presence and intensity of deformation affect the crystallization kinetics and rheology of lavas and magmas
- Measurements and models at thermodynamic equilibrium or without deformation are insufficient to describe natural transport processes
- Magmatic flow models require melt-composition-specific flow and crystallization models describing their rheologic solidification (T_{cutoff})

Supporting Information:
- Supporting Information S1
- Table S1
- Table S2
- Table S3
- Table S4
- Table S5
- Figure S1

Correspondence to:
S. Kolzenburg,
skolzenburg@gmail.com

Citation:
Kolzenburg, S., Giordano, D., Hess, K. U., & Dingwell, D. B. (2018). Shear rate-dependent disequilibrium rheology and dynamics of basalt solidification. *Geophysical Research Letters*, *45*, 6466–6475. https://doi.org/10.1029/2018GL077799

Received 7 MAR 2018
Accepted 16 JUN 2018
Accepted article online 25 JUN 2018
Published online 7 JUL 2018

Shear Rate-Dependent Disequilibrium Rheology and Dynamics of Basalt Solidification

S. Kolzenburg[1,2,3], D. Giordano[1], K. U. Hess[2], and D. B. Dingwell[2]

[1]Dipartimento di Scienze della Terra, Università degli Studi di Torino, Turin, Italy, [2]Department für Geo- und Umweltwissenschaften, Ludwig-Maximilians-Universität, Munich, Germany, [3]Department of Earth and Planetary Sciences, McGill University, Montreal, Quebec, Canada

Abstract Magmas and lavas undergo a range of shear rates during transport and emplacement. Further, transport of magma and lava occurs at subliquidus conditions where the melt crystallizes at varying temperature, pressure, and oxygen fugacity. Transport efficiency and eruption style are governed by magma rheology, which evolves during cooling, crystallization and degassing. Quantification of magma rheology rests almost exclusively on experimentation at constant temperature and shear rate. We present the first study on the effect of shear rate on subliquidus basalt rheology at conditions relevant to lava flows and shallow magmatic systems. The results reveal that basalts reach their rheologic *death* or cutoff temperature (T_{cutoff}; i.e., the point at which the sample rheologically solidifies and flow stops) at higher temperatures when flowing faster, whereas crystallization is suppressed when the shear rate is low. We explore the implications of shear-enhanced crystallization for modeling and forecasting of lava flow hazards and our understanding of magma and lava transport/storage systems.

Plain Language Summary Natural magmatic processes span several orders of magnitude in deformation rate. The presented approach is the first to systematically document the resulting effects on the magma/lava transport properties. Our paper presents an experimental study on the shear rate dependence of the crystallization/solidification dynamics and rheology of basalts at experimental conditions that mimic the natural environment. These were made possible through application of a newly developed experimental apparatus and method. The measurements show that at a specific subliquidus temperature, the so called *rheological cutoff temperature*, the effective viscosity of basalts increases dramatically, leading to solidification of the melt. Systematic investigation of this rheological cutoff shows a drastic, previously unrecognized, dependence on shear rate, cooling rate, and composition. High deformation rates result in more intense crystallization at higher temperatures, whereas crystallization is suppressed to lower temperatures in the absence of deformation. The presented results open an entirely new field of studies in magma rheology and have important implications for the forecasting of natural hazards, lava flow emplacement, and the understanding of magma and lava storage and transport systems in general. We discuss the implications of the experimental results for lava flow emplacement, magma migration, and for the computational modeling of lava flows for hazard assessment.

1. Introduction

Magma transport in the Earth's interior and lava transport on its surface typically occur at subliquidus conditions where the melts crystallize (Arzilli & Carroll, 2013; Kirkpatrick et al., 1981; Kolzenburg et al., 2017; Lofgren, 1980; Vetere et al., 2015). Transport efficiency, eruption style, and emplacement dynamics are governed by melt rheology (Chevrel et al., 2015; D. Giordano et al., 2007; Ishibashi, 2009; Vona & Romano, 2013), which evolves tremendously during cooling, deformation, and crystallization (Chevrel, Platz, et al., 2013; Kolzenburg et al., 2016; Vona et al., 2011). Despite the dynamic, subliquidus nature of magma and lava transport, quantification of their crystallization kinetics rests almost entirely on experiments performed without deformation and at constant temperature (Arzilli & Carroll, 2013; Cashman, 1993; Lange et al., 1994; Lofgren, 1980). Increasingly abundant data on equilibrium crystallization of natural melts have enabled the development of thermodynamic models such as MELTS (Gualda & Ghiorso, 2015). The conditions under which crystallization occurs in subvolcanic to volcanic systems are, however, transient, and disequilibrium is inherent. As a consequence, data and models based on equilibrium thermodynamics can only approximate the dynamics of magma and lava transport. This has inspired experimental studies at disequilibrium (Arzilli &

Carroll, 2013; Cashman, 1993; Kirkpatrick et al., 1981; Lange et al., 1994; Lofgren, 1980; Vetere et al., 2015). To date, however, deformation, as an experimental variable, has not been investigated.

Shear rates during transport in lava flows, dikes, conduit, and storage systems range from ~70 s^{-1} in Plinian eruptions (Papale, 1999), reach 2.5–0.001 s^{-1} in lava flows (Cashman et al., 2013; Kolzenburg et al., 2017, 2018; Piombo & Dragoni, 2009), and may go down to as low as 10^{-9} s^{-1} in magma chambers (Nicolas & Ildefonse, 1996). Magma ascent is associated with decreasing temperature and pressure and accompanied by degassing, crystallization, and changing oxygen fugacity (Applegarth et al., 2013; Kolzenburg et al., 2018; La Spina et al., 2015; Lipman et al., 1985), all of which strongly affect magma rheology. Cooling rates during the most common forms of magma ascent and lava flow range from tens of degrees per second in quench environments (D. Giordano et al., 2007; La Spina et al., 2015, 2016) to below 1°/hr in well-insulated flows (Kolzenburg et al., 2017; Witter & Harris, 2007) but may be higher or lower than this range in extremely thick or well-insulated lavas or during rapid heat loss, for example, in the presence of a cooling agent such as water.

Deformation-dependent crystallization is known for a variety of materials such as metallic glasses (Shao et al., 2015), plastic composites (Xu et al., 2011), and proteins (Azadani, 2007). Surprisingly, the deformation-dependent crystallization of magma/lava at conditions relevant to natural emplacement scenarios has not yet been experimentally investigated. Most studies of magma rheology are confined to constant temperature and shear rate (Chevrel et al., 2015; Ishibashi, 2009; Vona et al., 2011; Vona & Romano, 2013). Few studies investigate the rheology of cooling melts (D. Giordano et al., 2007; Kolzenburg et al., 2016, 2017, 2018). To date, only two studies discuss an influence of deformation on the crystallization of magma. Kouchi et al. (1986) show that nucleation rates and crystal number densities increase when deformation is applied and Vona and Romano (2013) compare the nucleation and growth rates of plagioclase and find that both increase with shear rate. Both studies were performed at constant temperature and cannot be directly applied to nonisothermal emplacement events.

Here we apply a multipronged experimental approach including classic concentric cylinder viscometry (CC-viscometry) for viscosity measurements, differential thermal analysis during viscometry (DTA-CC-viscometry) for measurement of viscosity and crystallization intensity in the presence of shear, and differential scanning calorimetry (DSC) for measurement of crystallization intensity in the absence of shear. These data are combined with textural analyses to systematically study the influence of shear rate on the rheological and petrological evolution of a crystallizing silicate melt at conditions relevant to dike and lava flow emplacement. The cooling and shear rates applied here span the widest range of experimentally accessible conditions (cooling rates of 0.5–3°C/min, shear rates from 4.64 to 0 s^{-1}, see also Kolzenburg et al., 2016; Kolzenburg et al., 2018, for details). This represents fast to intermediate cooling rates in volcanic conduits (La Spina et al., 2015, 2016), the interior of sheet-like lava flows and their crusts (Kolzenburg et al., 2017; Witter & Harris, 2007), and conditions of magma migration at shallow depths (D. Giordano et al., 2007; La Spina et al., 2015).

2. Materials and Methods

2.1. Sample Selection and Composition

Two melt compositions are chosen for this study: (1) a primitive basalt from the 2014–2015 eruption at Holuhraun, Iceland, and (2) a trachybasalt from Etna, Italy, sampled from the summit lava flow of the November 2013 eruption. These samples are representative of basaltic rift zone and subduction zone volcanism, respectively. The results presented here are, therefore, applicable to a wide range of volcanic environments associated to basaltic eruptions. The samples used in all the DTA-CC experiments are remelted and quenched to a glass after the end of the last experimental cycle. The chemical composition of the glasses is measured with a Cameca SX100 electron probe microanalyzer at LMU Munich. Analyses are carried out at 15-kV acceleration voltage, and, in order to minimize the alkali loss, a defocused beam (10 μm) and 5-nA beam current are used. Analytical procedures and normalized analysis results are presented in Text S1 (Pouchou & Pichoir, 1991) and Table S1 in the supporting information (SI), respectively. Standard deviations for all elements are less than ±2.5%.

2.2. Super-Liquidus CC Viscosity Measurements

Viscosity measurements are performed using the same setup and method described in (Kolzenburg et al., 2016). The samples are stirred in the CC viscometer in air at a constant temperature of 1346°C

for several hours to achieve chemical and thermal homogeneity. This is confirmed by constant torque and temperature readings. The furnace temperature is then decreased in steps of 25°C and held until a steady temperature and torque reading is achieved for each step (typically ~45 min). These data are used to recover the samples' superliquidus viscosity at each temperature step. The same samples used to measure pure liquid viscosity are also used for subliquidus experiments. Measurements are performed by imposing cooling rates of 0.5 and 1°C/min and varying initial shear rates of 1.161 and 4.642 s^{-1}.

2.3. In Situ DTA-CC

The DTA-CC setup allows in situ measurements of the sample temperature over the entire course of the experiment and is described in detail in Kolzenburg et al. (2016) and the SI. Crystallization of the samples occurs at temperatures below 1200°C, and the measured temperature departs to higher values than the temperature of the furnace. In order to estimate the intensity and nature of this departure, we extrapolate the linear cooling path of the melt and normalize the recorded sample temperatures to this extrapolation. This allows us to recover the ΔT between the crystallizing melt and the extrapolated cooling model. DTA during shear is restricted by the mechanical constraints of the viscometry measurements and, therefore, only possible until the point where the measurement torque limit of the device is reached. DTA at no shear conditions is performed over the entire cooling path.

2.4. High-Temperature DSC

Controlled cooling crystallization experiments at no shear conditions were performed in a Netzsch® DSC 404 C Pegasus DSC. Samples were heated to 1350°C and cooled at 3, 5, and 10°C/min. In these experiments the DSC is used as a high precision differential thermal analyzer for all measurements labeled DSC. Measurements are performed under a constant flow of argon gas using the same, lidded Pt-Rh crucibles (6 mm in diameter). For details on the sample preparation, measurement path, and data reduction please see the SI Text S3 (Giordano et al., 2015).

2.5. Glass Transition Measurements

Measurements of the glass transition temperature at onset (Tg_{onset}) and peak (Tg_{peak}) of the heat capacity curves are performed on separate samples of both the Etna and Holuhraun melts. These are undergoing cooling/heating cycles at rates of 10°C/min for the Holuhraun and 10 and 20°C/min for the Etna melt, respectively. Reproducibility of both Tg_{onset} and Tg_{peak} are better than 0.5% (i.e., 3°C). These data are used to recover the low temperature viscosity data using the method presented by Giordano et al. (2008). These data, together with the high T viscosity measurements, are used to recover the theoretical crystal-free liquid viscosity at subliquidus temperatures (see SI for details). Calculated data obtained by using this method are reported in Tables S2a and S2b together with their associated uncertainties.

2.6. Experiments for Textural Analysis

Experiments for textural analyses were performed only for the Holuhraun sample to give a qualitative overview of the influence of shear rate on paragenesis and texture. Rheological experimentation for the analysis of changes in sample texture as a function of shear rate is performed using a Brookfield DV-III+ viscometer head. Hand-crafted disposable spindles, similar to the ones described in Chevrel et al. (2015) are used for each experiment. For details on the measurement path and data treatment for measurements on both setups used here please see the SI Text S5 (Chevrel et al., 2015; Meerlender, 1975). In order to compare the textures in experiments with and without the presence of shear, we perform another experiment for textural analysis. This experiment is performed in the same experimental setup as outlined above but without introducing the spindle in the sample. We subject the sample to the same cooling path as the rheological experiments but without introducing deformation. Samples from experiments described in section 2.6 are embedded in epoxy resin and sectioned perpendicular to the rotation axis of the spindle. The samples are then polished and carbon coated for electron microscopy. Backscattered electron image maps are collected at 100X magnification using a JEOL JSM IT300LV scanning electron microscope at the University of Torino, Department of Earth Sciences.

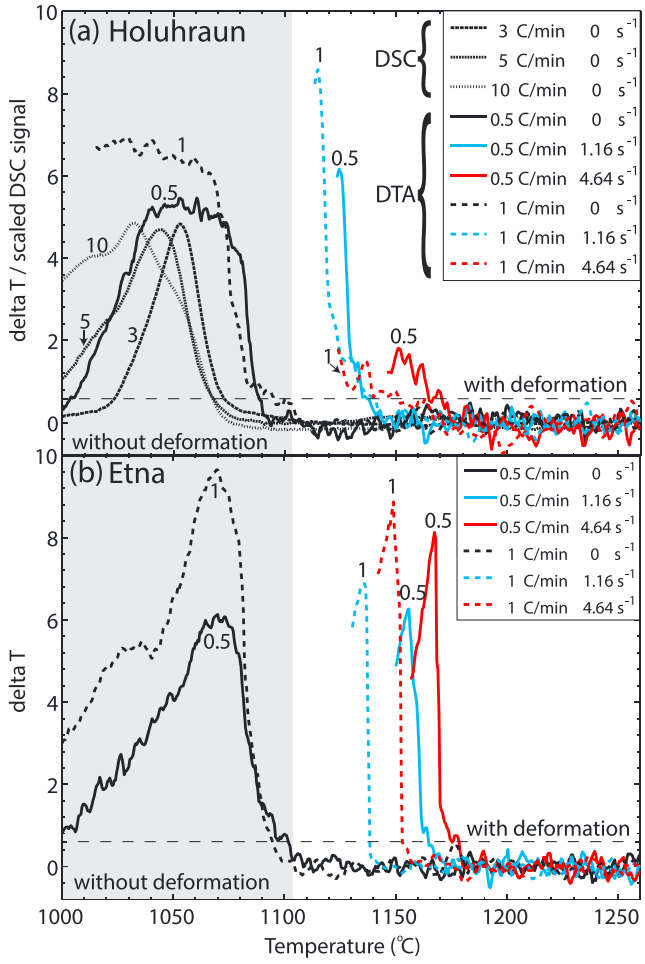

Figure 1. DSC and DTA data for Holuhraun (a) and Etna (b). (a) Solid and dashed red, blue, and black lines show DTA data (delta T in degrees Celsius) of the Holuhraun melt at 0.5 and 1°C/min and shear rates of 4.64, 1.16, and 0 s^{-1}, respectively. Small numbers on the curves are cooling rates. In the absence of shear (gray shaded areas) T_{onset} does not shift significantly with cooling rate. Crystallization onset T_{onset} increases with increasing shear rate. Dotted black lines show rescaled DSC data (see supporting information for data processing). (b) Solid and dashed red, blue, and black lines show the DTA data of the Etna melt at 0.5 and 1°C/min and shear rates of 4.64, 1.16, and 0 s^{-1}, respectively. The thin dashed line represents the threshold for determination of T_{onset} for the DTA-CC data. DSC = differential scanning calorimetry; DTA = differential thermal analysis; CC = concentric cylinder.

3. Results

3.1. DTA

The crystallization onset (T_{onset}) in the DSC data is defined as the departure from the baseline (delta T = 0). This is evaluated, analogous to T_{onset} in glass transition temperature measurements, by extrapolating the linear part of the increasing signal to the baseline. Due to the lower sensitivity and increased noise in the DTA-CC data, we define the crystallization onset (T_{onset}) for the DTA-CC data as the point where the signal exceeds the noise in the data ($\Delta T > 0.6$°C). Without shear, T_{onset} measured in the DSC apparatus for the Holuhraun sample is at the lowest temperature of all presented experiments (~1074 ± 2°C, Figure 1a). The peak crystallization intensity in the DSC experiments shifts to higher temperatures with decreasing cooling rate. This trend is also observable in the DTA data, where the crystallization peak is reached earlier for the cooling rate of 0.5°C/min than for the 1°C/min experiment. T_{onset} however shifts from 1088 to 1100°C for cooling rates of 0.5 and 1°C/min, respectively. The shift in T_{onset} between DSC and DTA data is likely related to both the changes in the cooling rate and changes in the surface to volume ratio between the two different methods. In the DSC setup, a small amount of the melt is in contact to a large crucible surface; this ratio allows for very detailed DTA analysis. In the CC-DTA setup, a large sample volume is in contact with a relatively small crucible surface. This difference in geometry likely induces also variations in the potential nucleation sites and distribution of surface tension within the sample and may, therefore, have some effect on T_{onset} of the melt. The overall temperature range of crystallization, however, is in good agreement between the two methods, and the DSC data are well reproduced by DTA data from experiments without shear in the CC setup.

When shear is introduced, the crystallization onset (T_{onset}) of the Holuhraun melt shifts to higher temperatures. At a cooling rate of 0.5°C/min T_{onset} increases by 50 and 83 to 1138 and 1171°C for shear rates of 1.16 and 4.64 s^{-1}, respectively. At a cooling rate of 1°C/min this shift is less pronounced, with T_{onset} increasing by 40 and 51 to 1140 and 1151°C for shear rates of 1.16 and 4.64 s^{-1}, respectively. Due to the technical challenges detailed in SI Text S3, DTA measurements for the Etna melt were restricted to the DTA-CC method. Without shear (Figure 1b) T_{onset} lies at 1101 and 1094°C for cooling rates of 0.5 and 1°C/min, respectively. At a cooling rate of 0.5°C/min T_{onset} increases by 63 and 77 to 1164 and 1178°C for shear rates of 1.16 and 4.64 s^{-1}, respectively. At a cooling rate of 1°C/min the shift is less pronounced, with T_{onset} increasing by 44 and 58 to 1138 and 1152°C for shear rates of 1.16 and 4.64 s^{-1}, respectively. This indicates that the effects of shear rate and cooling rate are not independent but, in fact, interdependent. For the Holuhraun melt, the shear rate dependence of the shift in T_{onset} decreases with increasing cooling rate (i.e., the shift is large at a cooling rate of 0.5°C/min and small at a cooling rate of 1°C/min). For the Etna melt this shift is large at both cooling rates, highlighting that important differences in the cooling and shear rate-dependent crystallization kinetics exist and that they vary with melt composition.

3.2. Viscometry

The results from the viscosity measurements are reported as relative viscosity in Figure 2. During crystallization, the composition of the residual melt changes due to the removal of certain components from the melt to form the crystals. However, any effect this may have on the residual melt viscosity and the data presented here is negligible. Details on how this was assessed as well as the data reduction are presented SI S1

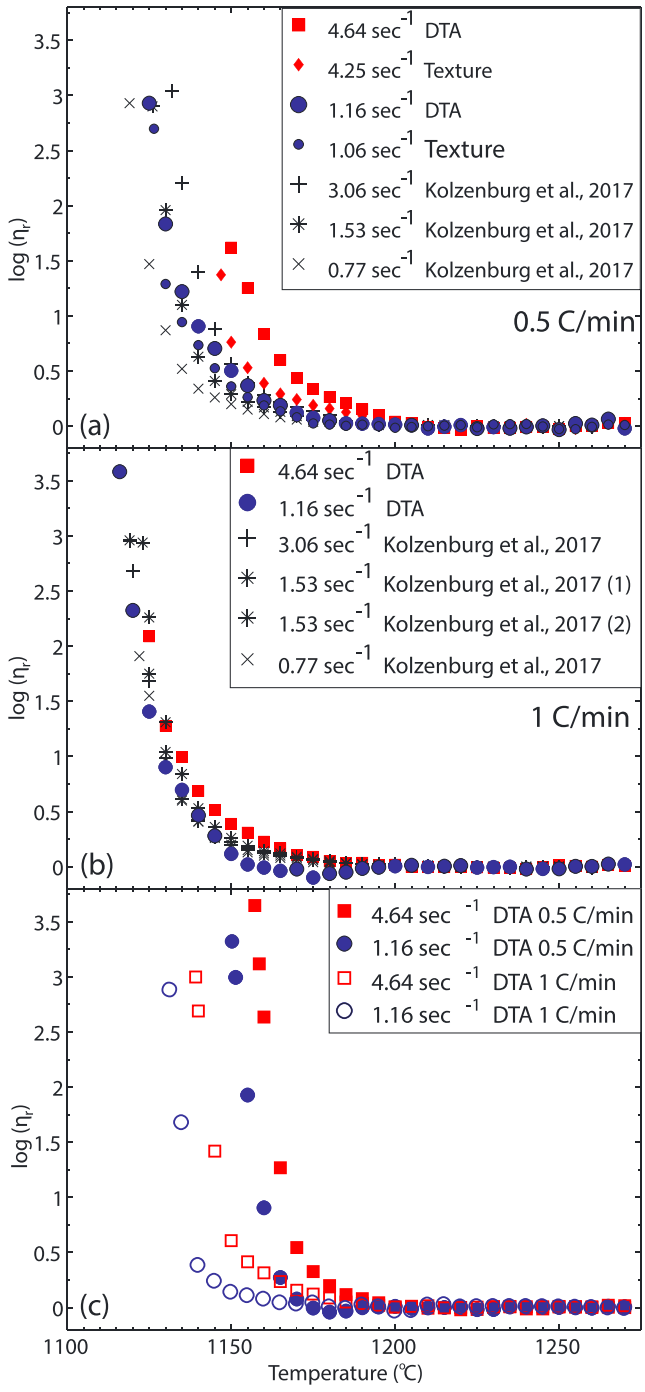

Figure 2. Rheological data plotted as log (η_r). (a) Holuhraun melt cooled at 0.5°C/min. Red squares and blue large circles are DTA-CC measurements; red diamonds and blue small circles are texture-CC measurements. Black plus, star, and cross are CC measurements from Kolzenburg et al. (2017); data labeled (1) and (2) are repeat measurements at the same shear rate. (b) Holuhraun melt cooled at 1°C/min. (c) Etna melt, red filled and open squares are DTA-CC data at 4.64 s^{-1} shear rate, cooled at 0.5 and 1°C/min, respectively. Blue filled and open circles are DTA-CC data at 1.16 s^{-1} shear rate, cooled at 0.5 and 1°C/min, respectively. DTA = differential thermal analysis; CC = concentric cylinder.

(Ghiorso & Sack, 1995; Giordano et al., 2008; Giordano & Dingwell, 2008; Tammann & Hesse, 1926). Any changes in relative viscosity and their variation with shear rate are therefore related to the effect of crystal nucleation and growth and their kinetics (i.e., increasing solid fraction in the suspension).

During cooling the viscosity initially follows the crystal-free liquid, resulting in a relative viscosity (log η_r) of zero. Below the liquidus, the data deviate from this trend at different degrees of undercooling until the system's rheological T_{cutoff} is reached, where the apparent viscosity of the suspension rises drastically, (i.e., it rheologically solidifies). This departure (increasing log η_r) varies with cooling and shear rate. For the Holuhraun melt (Figures 2a and 2b) we incorporate data from Kolzenburg et al. (2017) for comparison. Independent of measurement geometry, shear rate has a strong effect on T_{cutoff} of the Holuhraun melt at a cooling rate of 0.5°C/min. At a cooling rate of 1°C/min this effect is less pronounced indicating that the shear rate effect can be counterbalanced by changes in cooling rate, as suggested by the DTA data in Figure 1a. For the Etna melt (Figure 2 c) shear rate has a strong effect on T_{cutoff} of the crystallizing melt, independent of the cooling rate. Increased shear rates result in systematically increasing T_{cutoff}. Further, T_{cutoff} increases with increasing cooling rate.

3.3. Textural Analysis

The Holuhraun sample shows drastic changes in paragenesis and texture with shear rate (Figure 3). In the absence of shear, the dominant phase in this experiment is iron-rich spinel with subordinate clinopyroxene. The crystal habits are acicular dendritic to fibrous. Crystal widths are below ~10 μm and lengths vary from ~40 to 600 μm. At a shear rate of 1.16 s^{-1} the habits of the spinel crystals are radiating dendritic to reticulate. Crystal widths range from ~5 to 40 μm and lengths from ~10 to 700 μm. The habits of the clinopyroxene crystals are stubby. Crystal widths range from ~15 to 60 μm and lengths from ~20 to 90 μm. At a shear rate of 4.64 s^{-1} the habits of the plagioclase crystals are subhedral, columnar to prismatic, and hopper crystals are present. Crystal widths range from ~10 to 100 μm and lengths from ~50 to 750 μm. The habits of the spinel crystals are radiating dendritic to reticulate, and they often occur as clusters. Crystal widths range from ~10 to 80 μm and lengths from ~30 to 600 μm. Overall, the spinel crystal habits have lower aspect ratios at higher shear rates. The habits of the clinopyroxene crystals are elongate to stubby. Crystal widths range from ~5 to 20 μm and lengths from ~25 to 200 μm. The experimental samples do not show euhedral crystal shapes in any of the investigated cases. Crystallization in the absence of shear produces dendritic crystal habits, and they become more equilibrated (i.e., subhedral) with increasing deformation rate.

4. Discussion and Implications

4.1. Textural Evolution With Increasing Shear Rate

The textural variations reveal the influence of shear rate on the crystallization kinetics of natural melts. Crystal growth is hindered without shear (Figure 3a), because the melt around the growing crystal becomes depleted in the components required for further growth. This results in dendritic growth forms that are commonly observed in textural studies on the crystallization of basalts under cooling in the absence of shear

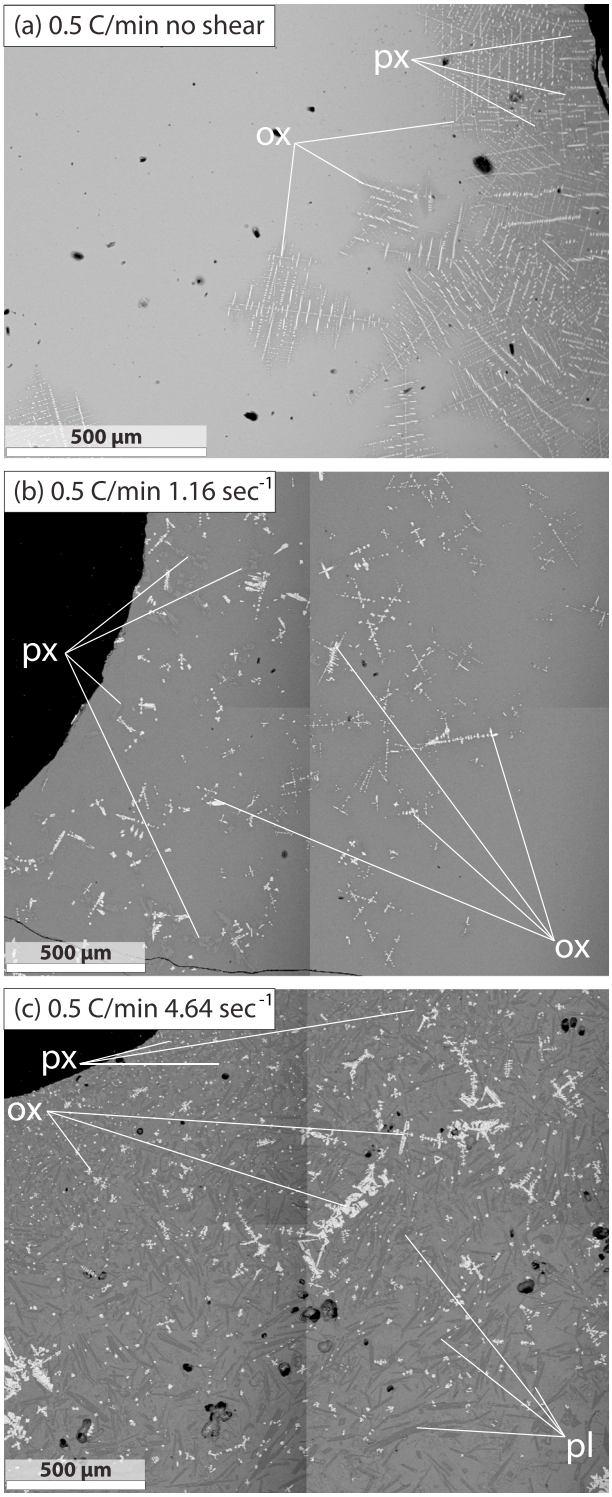

Figure 3. Textural analyses. Back-scattered electrons (BSE) photomicrographs of (a) Holuhraun melt cooled at 0.5°C/min without shear. Crystal habits are acicular, dendritic to fibrous, (b) Holuhraun melt cooled at 0.5°C/min at a shear rate of 1.16 s^{-1}. Crystal habits are stubby-arborescent to reticulated. (c) Holuhraun melt cooled at 0.5°C/min at a shear rate of 4.64 s^{-1}. Crystal habits are subhedral, columnar to prismatic. All samples were quenched at the same T = 1125°C.

(Kirkpatrick et al., 1981; Lofgren, 1980). These textural heterogeneities highlight that, although prediction of the solid fraction at a certain temperature and equilibrium conditions is possible through thermodynamic models, e.g., MELTS (Ghiorso & Sack, 1995; Gualda & Ghiorso, 2015), application of rheological models for suspensions, such as summarized in Mader et al. (2013), is not straightforward since the crystal habits vary greatly dependent on the applied deformation and cooling conditions. Once shear is introduced, advective processes transport *fresh* melt to the crystal surface, facilitating growth. This produces larger crystals and favors equilibrated crystal habits (subhedral versus acicular); see also Vona and Romano (2013) and Kouchi et al. (1986). This demonstrates that shear rate plays a larger role than previously thought in controlling the crystallization kinetics of basaltic melts, and surface-limited growth, as suggested by Kirkpatrick (1977), assumes a minor role.

4.2. Implications for Modeling of Magma Migration and Lava Flow Emplacement

Fixed thresholds are commonly used to determine whether a parcel in a flow model will behave solid (i.e., stop) or liquid (i.e., flow). Stopping criteria are reported as (1) crystal volume fractions (Cashman et al., 1999; Costa et al., 2009; Harris & Rowland, 2001; Lejeune & Richet, 1995; Marsh, 1981; Pinkerton & Stevenson, 1992; Rutter & Neumann, 1995; H. R. Shaw, 1969), (2) degrees of undercooling (Costa & Macedonio, 2005; Keszthelyi & Self, 1998), or (3) fixed temperatures (Costa & Macedonio, 2005; Del Negro et al., 2008; Hidaka et al., 2005; Hon et al., 1994; H. Shaw et al., 1968; Spataro et al., 2010). To standardize these stopping criteria, we convert them into temperatures. For fixed crystal contents we model the equivalent temperature using MELTS, and for fixed degrees of undercooling we calculate the respective temperature below the melt liquidus modeled with MELTS software. This allows assessing the difference in modeled runout distances between previous stopping criteria and the shear rate dependent T_{cutoff}. In order to systematically describe the influence of shear rate on the rheologic cutoff, we evaluate the temperatures at which each experimental dataset passes a viscosity threshold of 103.2 Pa·s (Figure S1). Beyond this point, all data sets reach the measurement limit within few degrees of cooling; that is, the sample rheologically solidifies (for shear rates of 4.25 and 4.64 the limit was reached before this point and therefore extrapolated values are used). We fit linear models to the shear rate dependence of T_{cutoff} (Figure S1) of the Holuhraun lava and model a scenario tracking the melt from eruption to solidification. For details on the limitations of the experimental method and the derived models please see SI section S2 (Bouhifd et al., 2004; Chevrel et al., 2018; Chevrel, Giordano, et al., 2013; *D* Dingwell, 1991; *D B* Dingwell & Mysen, 1985; Friedman et al., 1963; Holtz et al., 1995; Kolzenburg et al., 2018; Llewellin & Manga, 2005; Llewellin et al., 2002; Richet et al., 1996; Robert et al., 2008; Whittington et al., 2000).

As basic, simplified, assumptions we set (1) a cooling rate of 0.5 and 1°C/min, (2) a lava flow height of 3 m, (3) a simplified non-linear shear distribution (equation (1)) in the channel where 80% of shear occurs in the lower 40% of the channel following the approach presented in (Piombo & Dragoni, 2009), and (4) an eruptive temperature at the liquidus (1196°C, from MELTS by Gualda & Ghiorso, 2015).

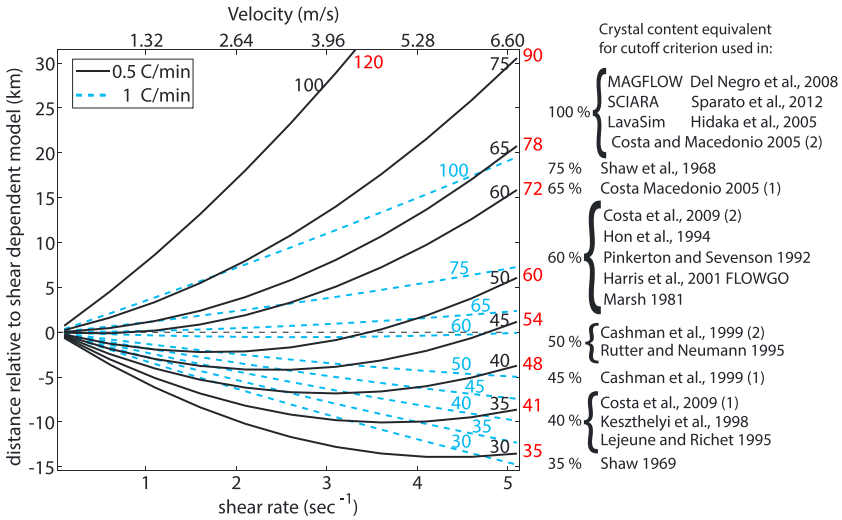

Figure 4. Implications for lava flow modeling. Simulations of flow length as a function of shear rate for the Holuhraun melt using a shear rate dependent halting criterion (T_{cutoff}). Results are presented relative to current halting criteria in flow models (black dashed line). Negative values mean underestimation (i.e., shorter L_{runout}); positive values mean overestimation of L_{runout}. Solid black and dashed blue lines are calculations for the shear rate dependence of T_{cutoff} at 0.5 and 1°C/min cooling rate, respectively. Black and blue numbers represent equilibrium crystal contents for the modeled temperatures at 0.5 and 1°C/min cooling rate, respectively. Red numbers show the degree of undercooling below melt liquidus for each curve of the 0.5°C/min cooling model. These numbers are identical for the correlating crystal content of the 1°C/min model. The legend shows which curves are representative of previous solidification criteria.

Based on these assumptions we calculate the surface velocity of the lava:

$$V_{surf} = (\dot{\epsilon}\times 0.8)\times(h\times 0.4) + (\dot{\epsilon}\times 0.2)\times(h\times 0.6) \quad (1)$$

where V_{surf} is the surface velocity in meters per second, $\dot{\epsilon}$ the shear rate in per second, and h the channel height in meters.

We calculate the cooling time in seconds (t_{flow}) to its T_{cutoff} from the difference between the eruptive temperature and the shear rate dependent T_{cutoff}:

$$t_{flow} = \frac{\Delta K}{\frac{\Delta T}{t}} \times 60 \quad (2)$$

where ΔK is the absolute difference between $T_{liquidus}$ and T_{cutoff} and $\Delta T/t$ the cooling rate in degrees Celsius per minute.

At constant velocity, this time t_{flow} in seconds equates to the distance (L_{runout}) in meters that the lava can flow before reaching T_{cutoff}, that is, solidifying.

$$L_{runout} = V_{surf} \times t_{flow} \quad (3)$$

Figure 4 shows the differences between the calculated runout distances of the shear dependent T_{cutoff} model and other stopping criteria. No previous stopping criterion accounts for shear rate-dependent crystallization, and, therefore, the predicted distances are linearly correlated to flow velocity. This linearity is lost when accounting for the shear rate dependence of T_{cutoff}, where higher shear rates result in higher T_{cutoff} and therefore shorter flow distances (see Figure 4). The model shows that the shear rate dependence of T_{cutoff} is small at a cooling rate of 1°C/min and higher at 0.5°C/min. Small variations in T_{cutoff} with shear rate result in quasi linear mismatches between the shear rate dependent runout distance and those calculated for previous stopping criteria. In fact, at 1°C/min, a 60% volume fraction of crystals gives satisfactory results.

At a cooling rate of 0.5°C/min, the effect of shear rate on runout distance becomes very pronounced. For stopping criteria up to ~40 vol% crystallinity, the runout distance is consistently underestimated. For 45 and 50 vol% crystallinity the runout distance is underestimated for low shear rates but overestimated at high shear rates. Stopping criteria above 60 vol% crystallinity consistently overestimate the runout distance.

Since all lavas cool in natural emplacement environments, lava flows will likely have lower than equilibrium crystal contents; see also Crisp and Baloga (1994). This is because the time needed to develop equilibrium crystal contents is not available as the melts are constantly driven to higher undercooling. Consequently, the temperature at which a given crystal volume fraction is present at disequilibrium is lower than modeled at equilibrium. The runout distances, therefore, represent minimum values. The actual distance is likely larger. This results in even larger discrepancies between the results of the new cooling and shear rate-dependent stopping criterion introduced here and current approaches. Incorporating T_{cutoff} measurements in lava flow models will allow for the concept of yield strength to be replaced by a melt-specific rheological T_{cutoff} that is both shear and cooling rate dependent. The concepts of yield strength or other arbitrary or empirically chosen parameters such as fixed crystal contents, temperature, or degrees of undercooling have been introduced in numerical simulations of lava flows (especially in cellular automata type models, e.g., Miyamoto & Sasaki, 1997) in order to ascribe a halting criterion to a modeled lava parcel. It has also been introduced as a rheologic criterion in planetary sciences for the derivation of rheological parameters from flow morphology, derived from experiments using analogue materials that possess yield strength (e.g., Fink & Griffiths, 1990; Hulme, 1974). In these analogue experiments these materials were chosen in order to mimic the development of a crust during cooling and not to represent actual flow rheology. T_{cutoff} data would therefore represent a more realistic description of the lavas rheological evolution and therewith better ability to forecast their emplacement.

The presented showcase model illustrates the effect of shear rate on the prediction of lava flow behavior, since the presented data, measured on degassed melts, at ambient pressure, equilibrated in air, are most applicable for such a scenario. However, shear rate will also play an important role in any magmatic system that is experiencing deformation at subliquidus conditions. Examples include convecting magma chambers, magma transport, and eruption feeder systems, fissure eruptions. It may also play a role in the efficiency of generating solidified and insulating flow carapaces and or lava tube systems. A quantitative assessment of the magnitude of the shear rate effect in such environments will require an extended experimental database mapping its importance as a function of composition and environmental parameters such as cooling rate and oxygen fugacity, since both have been shown to influence disequilibrium rheology (Kolzenburg et al., 2016, 2017, 2018).

5. Conclusions

In conclusion, we find the following:

1. Increased shear rates promote crystallization of magmas and lavas, which, in turn, affects their flow behavior. Therefore, magmas and lavas reach their T_{cutoff} or *rheologic death* at higher temperatures when flowing faster, whereas crystallization is suppressed to lower temperatures when the shear rate is low.
2. Measurements and models of magma rheology at thermodynamic equilibrium conditions or crystallization experiments without deformation are insufficient to describe natural transport processes. This highlights the need for the development of an empirical database mapping disequilibrium rheology in compositional, thermal, and shear rate space.
3. Modeling of magmatic flow behavior requires melt-composition-specific flow and crystallization models describing T_{cutoff} in order to provide more accurate results for lava flow hazard forecasting.

Acknowledgments
We thank W. Ertel-Ingrisch and C. Cimarelli for lab support. A. Höskuldsson, T. Throdarson, M. Coltelli, D. Andronico, and S. Calvari are thanked for field support. We further want to thank Leif Karlstrom and Oryaëlle Chevrel for their constructive reviews that helped make this manuscript more clear and concise. S. K. thanks the Westmount recreation center for providing an environment to balance the physical and mental requirements during data processing and writing. S. K. and D. G. acknowledge support from Fondazione CRT, Compagnia San Paolo, an ERASMUS Traineeship and the University of Torino. S. K. further acknowledges financial support from a H2020 Marie Skłodowska-Curie fellowship DYNAVOLC—795044. D. B. D. acknowledges ERC grant EVOKES—247076. All data are available in the supporting information (SI).

References

Applegarth, L., Tuffen, H., James, M., & Pinkerton, H. (2013). Degassing-driven crystallisation in basalts. *Earth-Science Reviews*, *116*, 1–16. https://doi.org/10.1016/j.earscirev.2012.10.007

Arzilli, F., & Carroll, M. R. (2013). Crystallization kinetics of alkali feldspars in cooling and decompression-induced crystallization experiments in trachytic melt. *Contributions to Mineralogy and Petrology*, *166*(4), 1011–1027. https://doi.org/10.1007/s00410-013-0906-1

Azadani, A. N. (2007). *Flow enhanced protein crystallization at the air/water interface*. ProQuest. Troy, New York: Rensselaer Polytechnic Institute.

Bouhifd, M. A., Richet, P., Besson, P., Roskosz, M., & Ingrin, J. (2004). Redox state, microstructure and viscosity of a partially crystallized basalt melt. *Earth and Planetary Science Letters*, *218*(1-2), 31–44. https://doi.org/10.1016/S0012-821X(03)00641-1

Cashman, K. V. (1993). Relationship between plagioclase crystallization and cooling rate in basaltic melts. *Contributions to Mineralogy and Petrology*, *113*(1), 126–142. https://doi.org/10.1007/BF00320836

Cashman, K. V., Soule, S., Mackey, B., Deligne, N., Deardorff, N., & Dietterich, H. (2013). How lava flows: New insights from applications of lidar technologies to lava flow studies. *Geosphere*, *9*(6), 1664–1680. https://doi.org/10.1130/GES00706.1

Cashman, K. V., Thornber, C., & Kauahikaua, J. P. (1999). Cooling and crystallization of lava in open channels, and the transition of Pāhoehoe Lava to ʻAʻā. *Bulletin of Volcanology*, *61*(5), 306–323. https://doi.org/10.1007/s004450050299

Chevrel, M. O., Cimarelli, C., deBiasi, L., Hanson, J. B., Lavallée, Y., Arzilli, F., & Dingwell, D. B. (2015). Viscosity measurements of crystallizing andesite from Tungurahua volcano (Ecuador). *Geochemistry, Geophysics, Geosystems*, *16*, 870–889. https://doi.org/10.1002/2014GC005661

Chevrel, M. O., Giordano, D., Potuzak, M., Courtial, P., & Dingwell, D. B. (2013). Physical properties of $CaAl_2Si_2O_8$–$CaMgSi_2O_6$–FeO–Fe_2O_3 melts: Analogues for extra-terrestrial basalt. *Chemical Geology*, *346*, 93–105. https://doi.org/10.1016/j.chemgeo.2012.09.004

Chevrel, M. O., Labroquère, J., Harris, A., & Rowland, S. (2018). PyFLOWGO: An open-source platform for simulation of channelized lava thermo-rheological properties. *Computers & Geosciences*, *111*, 167–180. https://doi.org/10.1016/j.cageo.2017.11.009

Chevrel, M. O., Platz, T., Hauber, E., Baratoux, D., Lavallée, Y., & Dingwell, D. B. (2013). Lava flow rheology: A comparison of morphological and petrological methods. *Earth and Planetary Science Letters*, *384*(0), 109–120. https://doi.org/10.1016/j.epsl.2013.09.022

Costa, A., Caricchi, L., & Bagdassarov, N. (2009). A model for the rheology of particle-bearing suspensions and partially molten rocks. *Geochemistry, Geophysics, Geosystems*, *10*, Q03010. https://doi.org/10.1029/2008GC002138

Costa, A., & Macedonio, G. (2005). Numerical simulation of lava flows based on depth-averaged equations. *Geophysical Research Letters*, *32*, L05304. https://doi.org/10.1029/2004GL021817

Crisp, J., & Baloga, S. (1994). Influence of crystallization and entrainment of cooler material on the emplacement of basaltic aa lava flows. *Journal of Geophysical Research*, *99*(B6), 11,819–11,831. https://doi.org/10.1029/94JB00134

Del Negro, C., Fortuna, L., Herault, A., & Vicari, A. (2008). Simulations of the 2004 lava flow at Etna volcano using the magflow cellular automata model. *Bulletin of Volcanology*, *70*(7), 805–812. https://doi.org/10.1007/s00445-007-0168-8

Dingwell, D. (1991). Redox viscometry of some Fe-bearing silicate melts. *American Mineralogist*, *76*(9–10), 1560–1562.

Dingwell, D. B., & Mysen, B. O. (1985). Effects of water and fluorine on the viscosity of albite melt at high pressure: A preliminary investigation. *Earth and Planetary Science Letters*, *74*(2-3), 266–274. https://doi.org/10.1016/0012-821X(85)90026-3

Fink, J. H., & Griffiths, R. W. (1990). Radial spreading of viscous-gravity currents with solidifying crust. *Journal of Fluid Mechanics*, *221*(1), 485–509. https://doi.org/10.1017/S0022112090003640

Friedman, I., Long, W., & Smith, R. L. (1963). Viscosity and water content of rhyolite glass. *Journal of Geophysical Research*, *68*(24), 6523–6535. https://doi.org/10.1029/JZ068i024p06523

Ghiorso, M. S., & Sack, R. O. (1995). Chemical mass transfer in magmatic processes IV. A revised and internally consistent thermodynamic model for the interpolation and extrapolation of liquid-solid equilibria in magmatic systems at elevated temperatures and pressures. *Contributions to Mineralogy and Petrology*, *119*(2–3), 197–212. https://doi.org/10.1007/BF00307281

Giordano, A., Nichols, M., Potuzak, D., Di Genova, C. R., & Russell, J. (2015). Heat capacity of hydrous trachybasalt from Mt Etna: Comparison with $CaAl_2Si_2O_8$ (An)–$CaMgSi_2O_6$ (Di) as basaltic proxy compositions. *Contributions to Mineralogy and Petrology*, *170*(5–6), 1–23.

Giordano, D., Polacci, M., Longo, A., Papale, P., Dingwell, D. B., Boschi, E., & Kasereka, M. (2007). Thermo-rheological magma control on the impact of highly fluid lava flows at Mt. Nyiragongo. *Geophysical Research Letters*, *34*, L06301. https://doi.org/10.1029/2006GL028459

Giordano, J. K. R., & Dingwell, D. B. (2008). Viscosity of magmatic liquids: A model. *Earth and Planetary Science Letters*, *271*(1–4), 123–134. https://doi.org/10.1016/j.epsl.2008.03.038

Giordano, M., Potuzak, C., Romano, D. B. D., & Nowak, M. (2008). Viscosity and glass transition temperature of hydrous melts in the system $CaAl_2Si_2O_8$–$CaMgSi_2O_6$. *Chemical Geology*, *256*(3–4), 203–215. https://doi.org/10.1016/j.chemgeo.2008.06.027

Gualda, G. A., & Ghiorso, M. S. (2015). MELTS_Excel: A Microsoft Excel-based MELTS interface for research and teaching of magma properties and evolution. *Geochemistry, Geophysics, Geosystems*, *16*, 315–324. https://doi.org/10.1002/2014GC005545

Harris, A. J., & Rowland, S. (2001). FLOWGO: A kinematic thermo-rheological model for lava flowing in a channel. *Bulletin of Volcanology*, *63*(1), 20–44. https://doi.org/10.1007/s004450000120

Hidaka, M., Goto, A., Umino, S., & Fujita, E. (2005). VTFS project: Development of the lava flow simulation code LavaSIM with a model for three-dimensional convection, spreading, and solidification. *Geochemistry, Geophysics, Geosystems*, *6*, Q07008. https://doi.org/10.1029/2004GC000869

Holtz, F., Behrens, H., Dingwell, D. B., & Johannes, W. (1995). H2O solubility in haplogranitic melts: Compositional, pressure, and temperature dependence. *American Mineralogist*, *80*(1–2), 94–108. https://doi.org/10.2138/am-1995-1-210

Hon, K., Kauahikaua, J., Denlinger, R., & Mackay, K. (1994). Emplacement and inflation of pahoehoe sheet flows: Observations and measurements of active lava flows on Kilauea Volcano, Hawaii. *Geological Society of America Bulletin*, *106*(3), 351–370. https://doi.org/10.1130/0016-7606(1994)106<0351:EAIOPS>2.3.CO;2

Hulme, G. (1974). The interpretation of lava flow morphology. *Geophysical Journal International*, *39*(2), 361–383. https://doi.org/10.1111/j.1365-246X.1974.tb05460.x

Ishibashi, H. (2009). Non-Newtonian behavior of plagioclase-bearing basaltic magma: Subliquidus viscosity measurement of the 1707 basalt of Fuji volcano, Japan. *Journal of Volcanology and Geothermal Research*, *181*(1–2), 78–88. https://doi.org/10.1016/j.jvolgeores.2009.01.004

Keszthelyi, L., & Self, S. (1998). Some physical requirements for the emplacement of long basaltic lava flows. *Journal of Geophysical Research*, *103*(B11), 27,447–27,464. https://doi.org/10.1029/98JB00606

Kirkpatrick, R. J. (1977). Nucleation and growth of plagioclase, Makaopuhi and Alae lava lakes, Kilauea Volcano, Hawaii. *Geological Society of America Bulletin*, *88*(1), 78–84. https://doi.org/10.1130/0016-7606(1977)88<78:NAGOPM>2.0.CO;2

Kirkpatrick, R. J., Kuo, L.-C., & Melchior, J. (1981). Crystal growth in incongruently-melting compositions; programmed cooling experiments with diopside. *American Mineralogist*, *66*(3–4), 223–241.

Kolzenburg, S., Jaenicke, J., Münzer, U., & Dingwell, D. B. (2018). The effect of inflation on the morphology-derived rheological parameters of lava flows and its implications for interpreting remote sensing data-A case study on the 2014/2015 eruption at Holuhraun, Iceland. *Journal of Volcanology and Geothermal Research*, *357*, 200–212.

Kolzenburg, S., Giordano, D., Cimarelli, C., & Dingwell, D. B. (2016). In situ thermal characterization of cooling/crystallizing lavas during rheology measurements and implications for lava flow emplacement. *Geochimica et Cosmochimica Acta*, *195*, 244–258. https://doi.org/10.1016/j.gca.2016.09.022

Kolzenburg, S., Giordano, D., Thordarson, T., Höskuldsson, A., & Dingwell, D. B. (2017). The rheological evolution of the 2014/2015 eruption at Holuhraun, Central Iceland. *Bulletin of Volcanology*, *79*(6), 45. https://doi.org/10.1007/s00445-017-1128-6

Kouchi, A., Tsuchiyama, A., & Sunagawa, I. (1986). Effect of stirring on crystallization kinetics of basalt: Texture and element partitioning. *Contributions to Mineralogy and Petrology*, *93*(4), 429–438. https://doi.org/10.1007/BF00371713

La Spina, G., Burton, M., & Vitturi, M. d. M. (2015). Temperature evolution during magma ascent in basaltic effusive eruptions: A numerical application to Stromboli volcano. *Earth and Planetary Science Letters*, *426*, 89–100.

La Spina G., Burton, M., Vitturi, M. d. M., & Arzilli, F. (2016). Role of syn-eruptive plagioclase disequilibrium crystallization in basaltic magma ascent dynamics, *Nature Communications*, *7*, 13402.

Lange, R. A., Cashman, K. V., & Navrotsky, A. (1994). Direct measurements of latent heat during crystallization and melting of a ugandite and an olivine basalt. *Contributions to Mineralogy and Petrology*, *118*(2), 169–181. https://doi.org/10.1007/BF01052867

Lejeune, A. M., & Richet, P. (1995). Rheology of crystal-bearing silicate melts: An experimental study at high viscosities. *Journal of Geophysical Research*, *100*(B3), 4215–4229. https://doi.org/10.1029/94JB02985
Lipman, P. W., Banks, N. G., & Rhodes, J. M. (1985). Degassing-induced crystallization of basaltic magma and effects on lava rheology. *Nature*, *317*(6038), 604–607. https://doi.org/10.1038/317604a0
Llewellin, E., Mader, H., & Wilson, S. (2002). The rheology of a bubbly liquid, paper presented at Proceedings of the Royal Society of London A: Mathematical, Physical and Engineering Sciences. *The Royal Society*, *458*(2020), 987–1016. https://doi.org/10.1098/rspa.2001.0924
Llewellin, E., & Manga, M. (2005). Bubble suspension rheology and implications for conduit flow. *Journal of Volcanology and Geothermal Research*, *143*(1-3), 205–217. https://doi.org/10.1016/j.jvolgeores.2004.09.018
Lofgren, G. (1980). Experimental studies on the dynamic crystallization of silicate melts. In R. B. Hargraves (Ed.), *Physics of magmatic processes* (pp. 487–551). Princeton, NJ: Princeton University.
Mader, H. M., Llewellin, E. W., & Mueller, S. P. (2013). The rheology of two-phase magmas: A review and analysis. *Journal of Volcanology and Geothermal Research*, *257*, 135–158. https://doi.org/10.1016/j.jvolgeores.2013.02.014
Marsh, B. (1981). On the crystallinity, probability of occurrence, and rheology of lava and magma. *Contributions to Mineralogy and Petrology*, *78*(1), 85–98. https://doi.org/10.1007/BF00371146
Meerlender, G. (1975). Erstes Standardglas der Deutschen Glastechnischen Gesellschaft und Realisierung der Viskositätsskala bei hohen Temperaturen. *Rheologica Acta*, *14*(3), 279–290. https://doi.org/10.1007/BF01515966
Miyamoto, H., & Sasaki, S. (1997). Simulating lava flows by an improved cellular automata method. *Computational Geosciences*, *23*(3), 283–292. https://doi.org/10.1016/S0098-3004(96)00089-1
Nicolas, A., & Ildefonse, B. (1996). Flow mechanism and viscosity in basaltic magma chambers. *Geophysical Research Letters*, *23*(16), 2013–2016. https://doi.org/10.1029/96GL02073
Papale, P. (1999). Strain-induced magma fragmentation in explosive eruptions. *Nature*, *397*(6718), 425–428. https://doi.org/10.1038/17109
Pinkerton, H., & Stevenson, R. J. (1992). Methods of determining the rheological properties of magmas at sub-liquidus temperatures. *Journal of Volcanology and Geothermal Research*, *53*(1–4), 47–66. https://doi.org/10.1016/0377-0273(92)90073-M
Piombo, A., & Dragoni, M. (2009). Evaluation of flow rate for a one-dimensional lava flow with power-law rheology. *Geophysical Research Letters*, *36*, L22306. https://doi.org/10.1029/2009GL041024
Pouchou, J. L., & Pichoir, F. (1991). Quantitative analysis of homogeneous or stratified microvolumes applying the model "PAP". In *Electron probe quantitation* (pp. 31–75). Boston, MA: Springer.
Richet, P., Lejeune, A.-M., Holtz, F., & Roux, J. (1996). Water and the viscosity of andesite melts. *Chemical Geology*, *128*(1-4), 185–197. https://doi.org/10.1016/0009-2541(95)00172-7
Robert, G., Russell, J. K., Giordano, D., & Romano, C. (2008). High-temperature deformation of volcanic materials in the presence of water. *American Mineralogist*, *93*(1), 74–80. https://doi.org/10.2138/am.2008.2665
Rutter, E., & Neumann, D. (1995). Experimental deformation of partially molten Westerly granite under fluid-absent conditions, with implications for the extraction of granitic magmas. *Journal of Geophysical Research*, *100*(B8), 15,697–15,715. https://doi.org/10.1029/94JB03388
Shao, Z., Singer, J. P., Liu, Y., Liu, Z., Li, H., Gopinadhan, M., et al. (2015). Shear-accelerated crystallization in a supercooled atomic liquid. *Physical Review E*, *91*(2), 020301. https://doi.org/10.1103/PhysRevE.91.020301
Shaw, H., Wright, T., Peck, D., & Okamura, R. (1968). The viscosity of basaltic magma; an analysis of field measurements in Makaopuhi lava lake, Hawaii. *American Journal of Science*, *266*(4), 225–264. https://doi.org/10.2475/ajs.266.4.225
Shaw, H. R. (1969). Rheology of basalt in the melting range. *Journal of Petrology*, *10*(3), 510–535. https://doi.org/10.1093/petrology/10.3.510
Spataro, W., Avolio, M. V., Lupiano, V., Trunfio, G. A., Rongo, R., & D'Ambrosio, D. (2010). The latest release of the lava flows simulation model SCIARA: First application to Mt Etna (Italy) and solution of the anisotropic flow direction problem on an ideal surface. *Procedia Computer Science*, *1*(1), 17–26. https://doi.org/10.1016/j.procs.2010.04.004
Tammann, G., & Hesse, W. (1926). Die Abhängigkeit der Viscosität von der Temperatur bie unterkühlten Flüssigkeiten. *Zeitschrift für Anorganische und Allgemeine Chemie*, *156*(1), 245–257. https://doi.org/10.1002/zaac.19261560121
Vetere, F., Iezzi, G., Behrens, H., Holtz, F., Ventura, G., Misiti, V., et al. (2015). Glass forming ability and crystallisation behaviour of sub-alkaline silicate melts. *Earth-Science Reviews*, *150*, 25–44. https://doi.org/10.1016/j.earscirev.2015.07.001
Vona, A., & Romano, C. (2013). The effects of undercooling and deformation rates on the crystallization kinetics of Stromboli and Etna basalts. *Contributions to Mineralogy and Petrology*, *166*(2), 491–509. https://doi.org/10.1007/s00410-013-0887-0
Vona, A., Romano, C., Dingwell, D. B., & Giordano, D. (2011). The rheology of crystal-bearing basaltic magmas from Stromboli and Etna. *Geochimica et Cosmochimica Acta*, *75*(11), 3214–3236. https://doi.org/10.1016/j.gca.2011.03.031
Whittington, A., Richet, P., & Holtz, F. (2000). Water and the viscosity of depolymerized aluminosilicate melts. *Geochimica et Cosmochimica Acta*, *64*(21), 3725–3736. https://doi.org/10.1016/S0016-7037(00)00448-8
Witter, J. B., & Harris, A. J. (2007). Field measurements of heat loss from skylights and lava tube systems. *Journal of Geophysical Research*, *112*, B01203. https://doi.org/10.1029/2005JB003800
Xu, J.-Z., Chen, C., Wang, Y., Tang, H., Li, Z.-M., & Hsiao, B. S. (2011). Graphene nanosheets and shear flow induced crystallization in isotactic polypropylene nanocomposites. *Macromolecules*, *44*(8), 2808–2818. https://doi.org/10.1021/ma1028104